CARBON 47 (2009) 3295–3305

available at www.sciencedirect.com

ScienceDirect

journal homepage: www.elsevier.com/locate/carbon

Characterization of circumstellar carbonaceous dust analogues produced by pyrolysis of acetylene in a porous graphite reactor

Ludovic Biennier [a,*], *Robert Georges* [a], *Vijayanand Chandrasekaran* [a], *Bertrand Rowe* [a], *Thierry Bataille* [b], *V. Jayaram* [c], *K.P.J. Reddy* [d], *E. Arunan* [e]

[a] *Astrochimie expérimentale, Institut de Physique de Rennes, Université de Rennes 1, UMR CNRS 6251, 35042 Rennes, France*
[b] *Sciences Chimiques de Rennes, Université de Rennes 1, UMR CNRS 6226, 35042 Rennes, France*
[c] *Solid State and Structural Chemistry Unit, Indian Institute of Science, 560012 Bangalore, India*
[d] *Department of Aerospace Engineering, Indian Institute of Science, 560012 Bangalore, India*
[e] *Inorganic and Physical Chemistry, Indian Institute of Science, 560012 Bangalore, India*

ARTICLE INFO

Article history:
Received 20 March 2009
Accepted 27 July 2009
Available online 6 August 2009

ABSTRACT

Carbon particles synthesized by acetylene pyrolysis in a porous graphite reactor have been investigated. The intimate chemical and physical structures of the particles were probed by proton nuclear magnetic resonance spectroscopy, infrared Fourier transform spectroscopy and X-ray diffraction. The analysis points towards a chemical structure composed of soluble low-mass aromatics surrounding small insoluble larger aromatic islands bridged by aliphatic groups. The diffraction profile indicates that the particles are mostly amorphous with small crystalline domains of ~6.5 Å composed of a few stacked graphene layers. The properties of these particles are compared with these obtained with other types of production methods such as laser pyrolysis and combustion flames. The results are briefly discussed in the context of the evolution of infrared interstellar emitters. Possible uses of the reactor are proposed.

1. Introduction

Across the Universe, astronomers observe a characteristic infrared signature with features peaking at 3.3, 6.2, 7.7, 8.6, 11.3 and 12.7 μm first discovered in the 70s [1]. These infrared emission bands, often accompanied by broad plateaus underneath them, are detected in a large number of stellar sources such as proto-planetary nebulae (PPNe), planetary nebulae (PNe), reflection nebulae, H II regions, young stellar objects and galaxies subjected to UV or visible excitation. The infrared features have been assigned to molecular emitters such as polycyclic aromatic hydrocarbons (PAHs) [2–4] and solid-state particles such as hydrogenated amorphous carbon grains [5], coal [6], quenched carbonaceous composites [7]. These compounds are believed to be dominantly produced in circumstellar envelopes of carbon-rich stars in the red giant and asymptotic giant branch (AGB) phases of their evolution [8]. Remarkably, the infrared bands remain absent from the spectrum of AGB stars. In the widespread view, the building blocks of carbon particles in those massive dust factories are assumed to be PAHs. Some insights into the poorly known formation mechanisms of carbon dust were given by combustion modelers who introduced chemistry into the envelopes [8], until then described by thermochemistry. The temperature and the chemical composition of combustion flames and pyrolysis environments are very close to those

* *Corresponding author:* Fax: +33 2 23 23 67 86.
E-mail address: ludovic.biennier@univ-rennes1.fr (L. Biennier).
0008-6223/$ - see front matter © 2009 Elsevier Ltd. All rights reserved.
doi:10.1016/j.carbon.2009.07.050

encountered in the photospheres of carbon-rich stars. Acetylene is the dominant carbon bearing molecule after carbon monoxide in circumstellar shells characterized by temperatures of about 2000 K. This similarity led Frenklach and Feigelson to apply a chemical model of PAH formation to the circumstellar envelopes of carbon-rich stars in late phases of their evolution [8]. This work was pursued by Cherchneff et al. [9–11] who studied the formation of PAHs in the inner envelope of such circumstellar shells, taking into account the effect of periodic shocks which are known to be present in the inner wind of AGB stars. A wider step was made later on, in which PAHs were proposed to stick to form dust nuclei across the shell [12].

In combustion flames, the process starts with the breakdown of a fraction of the fuel into smaller reactive molecules and radicals. The subsequent steps involve radical chains such as CH_3, n-C_4H_3, n-C_4H_5, and propargyl C_3H_3. From there different scenarios have been built. The dominant one supported by Frenklach leads to the formation of the first aromatic ring perceived as the rate limiting step. Two chemical routes have been singled out. The first one is an even carbon pathway that involves the addition of acetylene to n-C_4H_3 or n-C_4H_5 [13]. Because it was argued that these two radicals may not be present in sufficient amount as they transform rapidly into their isomers, an alternative odd carbon pathway which involves two propargyl radicals was proposed. According to Frenklach, once the first ring (C_6H_6) is formed, the aromatics grow by sequences of H abstraction followed by acetylene addition (HACA). In this picture, the phenyl radical (C_6H_5) which reacts with acetylene to form phenylacetylene represents a key intermediate towards the formation of multiple cyclic structures. The transition of gas phase species to solid particles is achieved by the formation of a critical nucleus composed of two PAHs above the size of pyrene. PAH dimers, held by van der Waals forces, collide with PAH molecules forming PAH trimers or with other dimers forming PAH tetramers, and so on, all while individual PAH species keep increasing in size via molecular chemical growth reactions. The core of this model is the accumulation of particle mass via chemical reactions with gaseous precursors simultaneously with the growth of particle size by collisions among PAH molecular species and clusters. Surface reactions involving acetylene and coagulation play a key role in the growth of the particles. Recent experiments by Sabbah et al. [14] have however seriously undermined the particle nucleation stage of the model by showing that pyrene molecules do not condense efficiently at temperatures characteristic of combustion environments (>1000 K). These results clearly show that major revision of the nucleation stage of the model is necessary.

The formation of carbonaceous particles may also proceed along other routes that may co-exist depending on the physical conditions. Early hints were given by non-equilibrium chemical kinetic calculations developed to explain the formation of meteoritic kerogen material, a cross linked structure of aliphatic and aromatic hydrocarbons [15]. The initial experimental evidence for such structures were reported by D'Anna et al. [16] and Dobbins and Subramaniasivam [17]. The results suggested a fast polymerization process the building bricks of which were aromatic compounds with few condensed rings connected by aliphatic bonds. In this picture confirmed by other studies [18], small hydrocarbon molecules, in particular acetylene, adds to radical chains to produce unsaturated hydrocarbon radicals that condense and give rise to the first particles. These primary particles generated through the process dubbed chemical condensation, consist of chain-like aggregates held by covalent bonds, not by van der Waals forces. These transparent particles in the visible may be more or less liquid and they may contain small aromatic moieties, interconnected by flexible hydrocarbon chains. The observation of liquid aromatic droplets has also been reported in a study of an acetylene diffusion flame via real-time aerosol mass spectrometry [19]. The heating of the particles in the flame first converts the aliphatic chains composing the structure into aromatic rings and then produces large arrays of aromatic rings that graphitize. The surface of the particle promotes PAH synthesis that may desorb from their surface [18]. Under this description, which awaits further investigation, PAHs are mainly by-products of the particles. The argument over formation routes is still going on as experimental studies of Grotheer et al. [20] indicate stacks of condensed PAHs as soot precursors under some conditions and nano organic carbon according to D'Anna et al. at others [21]. In summary the emerging picture seems to point out to a two pathway mechanism: the *high mass* PAH stacking route (the small ones hardly condensing at high temperatures) and aliphatic aromatic chemical growth.

Spatially resolved astronomical observations in the mid-infrared of the further stages of AGB star evolution i.e., PPNe and PNe also call for a revision of the picture of aromatic growth combining chemical reactions (extension of the ring skeleton) and physical processes (stacking of aromatics). Observations, supported by laboratory experiments [22], suggest that dust particles produced in the envelopes may be quite different from stacked PAHs and contain a strong aliphatic component. Amorphous hydrogenated carbon (a:C–H) consisting of islands of aromatic (sp^2) bonded C atoms joined together with a variety of peripheral sp^2 and sp^3 bonded hydrocarbons could represent a good candidate. The upper end of the size distribution of these grains may then provide the source for the smaller aromatic-rich species through fragmentation and photo-processing in the interstellar medium (e.g. [23]). The aliphatic to aromatic conversion of the circumstellar dust from PPNe to PNe correlates with a raise in stellar temperature, a less protective dusty environment, and harsh UV radiation [24].

Laboratory data on the kinetics of reactions involved in the growth of dust particles, the spectroscopy of the intermediate chemical species and the end-products, and the chemical and physical properties of the particles are critical to progress in our understanding of this ubiquitous component of space. A great variety of reactors have been used to produce astrophysical analogues of carbon particles. These include premixed [25], diffusion [22] and atmospheric [26] flames, laser induced pyrolysis of hydrocarbon mixtures [27–29], methane plasma deposition [30,31], laser ablation of graphite targets [32,33], and arc-discharge between carbon electrodes in rarefied atmosphere [26] following the pioneering work of Kroto et al. on fullerenes [34]. Post-condensation processes were also

simulated such as thermal annealing, ultraviolet irradiation, ion bombardment and exposure to atomic hydrogen [33,35].

The production and processing of carbon particles encompass a number of chemical and physical processes. These include gas phase neutral–neutral, ion–molecule and electron–ion reactions – covering a wide temperature range, surface chemistry, photodissociation, and photoionization. This also reflects the diversity of the environments encountered by a particle during its lifetime in space.

In this paper we will describe in Section 2 a new compact reactor to produce circumstellar analogues of carbonaceous particles from the pyrolysis of acetylene at high temperature. The chemical and physical characterization of the particles using proton NMR, infrared spectroscopy and X-ray diffraction, are detailed in Section 3. We conclude by discussing briefly the results, the techniques applied to characterize the analogues, the perspectives of this work, and possible uses of the reactor.

2. Production of carbonaceous particles

The production of carbonaceous particles is achieved by pyrolysis of acetylene in a unique versatile highly compact source. The circumstellar carbon analogues source, depicted in Fig. 1, is designed to be implemented in a 50 cm diameter vacuum chamber. It is interfaced to a high resolution Fourier transform spectrometer and used as a high temperature reactor of gaseous species such as hot methane [36].

The reduced dimension of the prototype is made possible by the use of a heated graphite rod whose open porosity provides a huge exchange surface and thus a very efficient heat transfer from the high temperature rod to the gas circulating through it. During the testing period of the prototype, temperatures of 1800 K were maintained for hours with mass flow rates of $Q_m \sim 0.6\ g\ s^{-1}$ of argon. The "furnace" is a cylindrical cavity drilled over almost the complete length of the graphite rod (outer diameter: $\varphi_O = 14$ mm, inner diameter, $\varphi_I = 8$ mm, length: 200 mm). The rod can be electrically heated up to 2000 K. It is maintained between two non-porous carbon electrodes inside a refractory jacket of tantalum. One end of the cylindrical piece of tantalum is connected to a reservoir supplied with acetylene. The other end of the jacket is connected to a chamber kept at low pressure ($5–30 \times 10^{-3}$ hPa) by means of a set of roots pumps. The gas is first passed through a cold zeolite trap maintained at 233 K before entering the reservoir to eliminate acetone contained in the bottle (Air Liquide, 99.7% purity). The jacket is supplied continuously by a small flow ($Q_v = 2.9$ liter min^{-1} atm [slm]) of cold acetylene regulated by a mass flow controller. The gas is heated up by passing through the high temperature porous walls of the graphite rod before ending its course in the rod cavity. It is then evacuated into the vacuum chamber where it expands supersonically. The radial migration of the molecules through the heating graphite walls leads to a good temperature uniformity along the whole length of the cavity. In the case of a conventional heated tube into which a cold gas is injected by one of its ends, a temperature gradient zone develops before the gas reaches a final temperature. In this study, such perturbing effect is avoided as the gas fills continuously the cavity from its periphery to its axis. The absence of temperature gradients is evidenced by the good linearity of the conventional Boltzmann plots used to extract the temperature from the rovibrational intensities of the $1 \rightarrow 0$ emission band of CO premixed with the C_2H_2 gaseous sample (0.1 slm). The jacket of tantalum is surrounded by a water cooled thermal shield whose internal face is coated with gold for reflecting the emitted radiations towards the high temperature source and then increasing its efficiency.

A CaF_2 wedged window is located in front of the exhaust of the emitting cavity to isolate the FT-IR spectroscopy interface

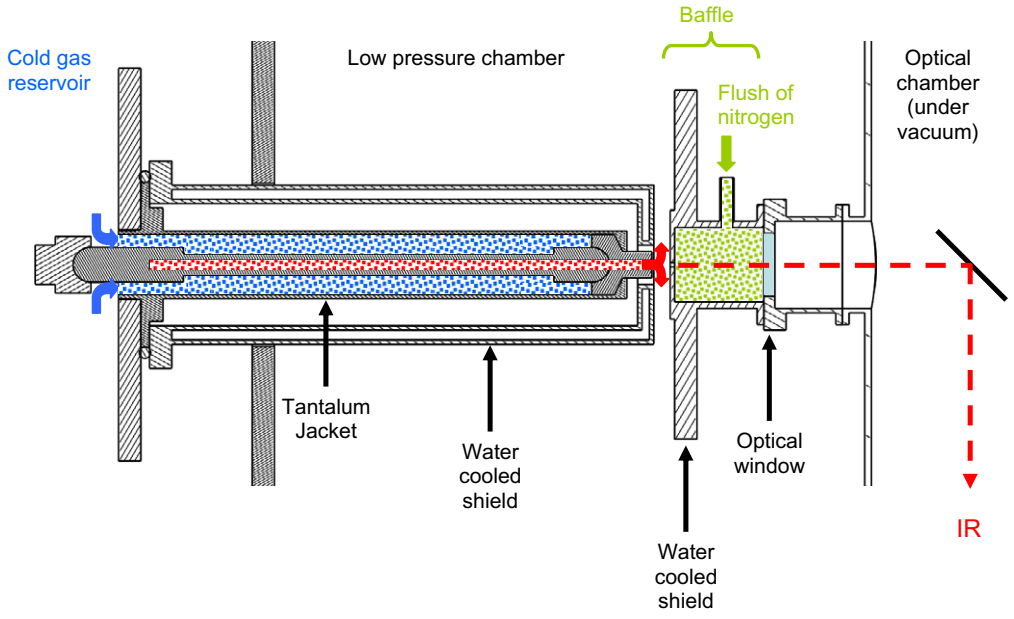

Fig. 1 – Circumstellar carbon analogues reactor. The source is coupled to a FT-IR spectrometer through its spectroscopy interface.

from the experimental chamber. The CaF_2 window is protected from the high temperature gas flow by a foil of tantalum fixed on water cooled support. A two mm hole bored in the foil reduces the sight solid angle and therefore limits the infrared light emitted by the graphite walls which could lead to saturation of the detector.

The efficiency of the heat exchange can be assessed by comparing the power dissipated by the resistor, $R(T)\ I^2$, and the power used to heat the gas, $Q_m\ c_p\ (T - T_0)$, with $R(T)$, the graphite rod resistance, I, the current flowing through the rod, c_p, the specific heat capacity at constant pressure, T, the final temperature, T_0, the initial temperature of the gas. The temperature of the flow in the central hollow channel of the graphite rod is derived from the analysis of the infrared emission band of CO following a procedure fully described in Ref. [36]. The resistance of the rod is determined by four point probe resistivity measurements over the 300–1100 K range. It appears to slightly increase with the temperature above 750 K because of thermal agitation and is extrapolated to ~0.35 Ω at 1400 K. For an applied current of 40 A, the power dissipated in the rod is therefore ~560 W, one-fifth of which effectively used to heat the flowing acetylene gas. A significant fraction of the power is lost by radiative and convective transfer to the tantalum jacket.

Fig. 2 shows the evolution of the 3 μm infrared emission spectrum of acetylene against the applied current. The intensity of the emission band for an optically thin medium follows Planck's law according to the relationship, $I \propto L^0 \sigma n l$, with L^0 the black body brightness, σ the absorption cross section, n the number density of the emitting molecules, and l the length of the emitting medium in the line of sight of the detector.

The rise of the black body brightness L^0 with temperature is moderated by the collapse of the absorption cross section, σ. As the net balance remains positive, it is expected that the emission intensity increases with the temperature. The high resolution emission spectra displayed in Fig. 2 reveal that this is not the case. The top panel clearly shows that the gas temperature – in thermal equilibrium in the cavity with the graphite rod – steadily rises with the current up to the value of ~40 A above which it attains a plateau. This behavior cannot be explained by the optical thickening of the emitting medium. This is interpreted as dissociation of a fraction of acetylene (drop of the number density of acetylene molecules) and explains the level off of the temperature as the extra energy is consumed to break the molecules and not to heat the gas further. It is worth noting that in a similar experiment, Mendiara et al., observed that around 86% of acetylene is converted into particles at the temperature of 1373 K [37]. Not surprisingly, the dissociation process is amplified when the dissipated electrical power is increased.

The particles are generated by pyrolysis of acetylene at ~1400 K during its residence time in the pores of the graphite rod. The residence time is given by $\frac{(\phi_0 - \phi_1)}{Q_V \times \frac{T}{298\ K} \frac{1\ atm}{P_{res}} \times A}$ with A the whole section traversed by the gas. It is evaluated to be around 6.5 ms for a reservoir pressure p_{res} of 100 mbar and temperatures T close to 1400 K. Once in the central channel, the particles are entrained in the vacuum chamber, cooled down in the supersonic expansion, hence freezing further

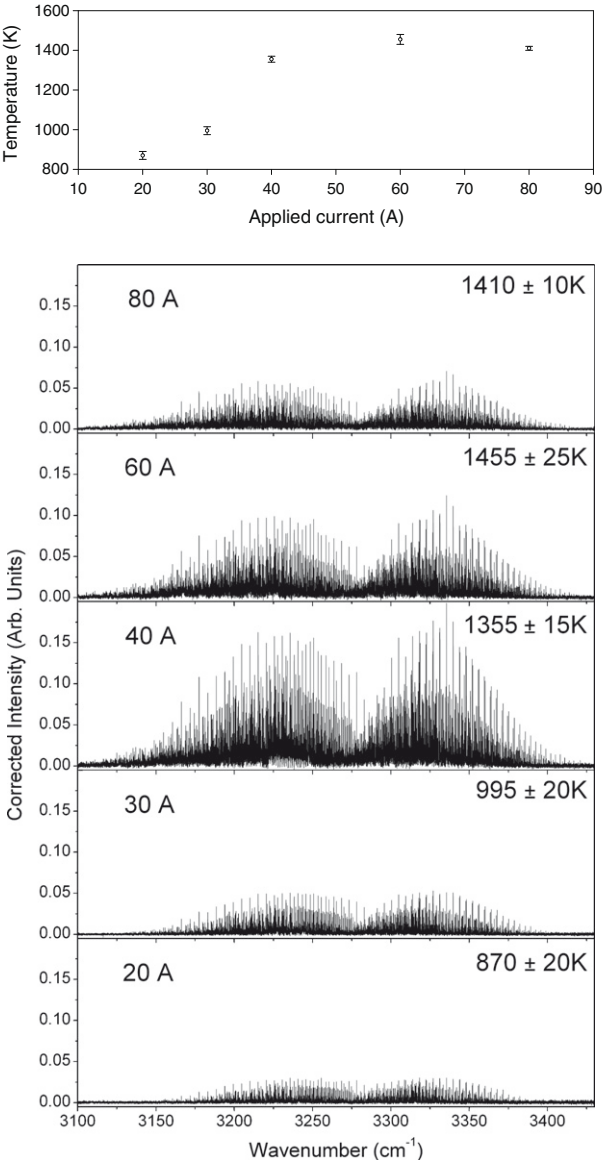

Fig. 2 – Bottom panel: high resolution (0.015 cm^{-1}) Fourier transform infrared emission spectrum of gaseous acetylene in the 3 μm region recorded for various applied electric currents increasing from the bottom to the top of the figure. The spectral intensities have been corrected from the apparatus transmission function. The temperature is determined by conventional Boltzmann plots of the rovibrational intensities of the 1 → 0 emission band of CO premixed to acetylene. Top panel: flow temperature vs. the applied current.

chemical reactions, and deposited onto the cooled shield protecting the optical window of the gas phase infrared spectroscopy interface.

The particles are then collected for further analysis to reveal their intimate chemical and physical structures. In this work, we use three different ex situ characterization techniques namely proton NMR, infrared spectroscopy and X-ray diffraction, that have all proven to be very helpful in the determination of the structure of particles.

3. Characterization

3.1. ^1H NMR

Proton nuclear magnetic resonance (NMR) spectroscopy is a tool routinely used for structural analysis of molecules by chemists. The NMR chemical shift allows for distinguishing magnetically inequivalent protons in a molecule. This technique has been employed to study soot particles produced during combustion [38]. The carbon sample, produced by pyrolysis of acetylene in the porous graphite reactor, is dissolved in deuterated chloroform $CDCl_3$, containing trace amounts of tetramethylsilane (TMS) used as an internal chemical shift reference. About 80% in mass of the material is dissolved. The ^1H NMR spectrum of the soluble fraction of the sample is recorded by a spectrometer operating at 200.13 MHz. The spectrum displayed in Fig. 3 bears some strong similarity with the spectrum of soot particles collected in an inverse diffusion flame [38].

The 7–9 ppm chemical shift region of the spectrum reveals the aromaticity of the material. A remarkable feature is the domination of only one aliphatic hydrogen peak, corresponding to a hydrogen atom in a methyl ($-CH_3$) or methylene group ($-CH_2$) attached to an aromatic ring. Only two very small peaks at 0.9 and 1.3 ppm are also attributed to hydrogen atoms in CH_3 groups attached to aliphatic carbons. Of interest is the absence of olefinic $-\dot{C}=\dot{C}-H$ protons (4.0–6.0 ppm) that are discernible in young soot particles. The analysis shows that the ratio of the integrated aromatic hydrogen broad peak to the H_α aliphatic hydrogen peak is about 8.1. This value is comparable to what is found for evolved soot particles. The explanation which has been elaborated for describing the evolution of soot particles in combustion is that particles carbonize with reaction time (or height above the burner) and aliphatic structures convert into aromatic subunits upon loss of hydrogen atoms, leading to more compact particles. We can assume that a similar mechanism is operating in the flow produced by the graphite rod source.

Although it is elusive to identify a single chemical species from such a spectrum that results from the contribution of hundreds of compounds, a search in proton NMR database shows that the small peak centered at 3.01 ppm combined with the absence of signal in the 3.1–6.5 ppm region is found in only a few hydrocarbon species including phenylacetylene which contains an acetylenic hydrogen. Although phenylacetylene is involved in the synthesis of the first PAHs in hot environments, it has not been detected so far. The presence of this peak may indicate that the material contains alkyl (C≡C) groups.

3.2. *FT-IR spectroscopy*

The infrared absorption spectrum of the carbon condensate mixed with KBr powder and pressed into a pellet is measured in transmission over the 400–4000 cm^{-1} region by a Spectrum-1000 Perkin Elmer Fourier transform infrared spectrometer with a resolution of 4 cm^{-1}. The infrared spectrum, displayed in Fig. 4, shows a series of intense well defined absorption features.

The identification of the main peaks has been done using previous studies (see Refs. [4,39] for instance) on laboratory analogues of carbon dust grains, soot and PAHs, and is recalled in Table 1. The sample displays characteristic strong aromatic features at 3.29 μm, (CH stretch), 6.30 μm (sp^2 C=C stretch) and 11.36, 11.98 and 13.31 μm (CH out of aromatic plane bending). These features are accompanied by a 7.7–10 μm broad component that is assigned to CC and CH plane deformation of aromatic groups. The presence of aliphatic groups i.e., CH_3–, $-CH_2-$, and =CH– bonded to or bridging aromatic rings in the material is evidenced by the 3.42 and 3.50 μm peaks, identified as aliphatic asymmetric and symmetric stretches.

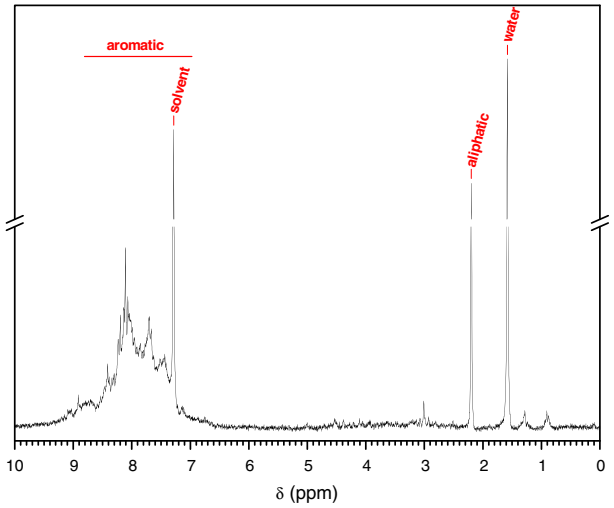

Fig. 3 – Proton NMR spectrum of the soluble fraction of the carbonaceous material produced by pyrolysis of acetylene in the porous graphite reactor.

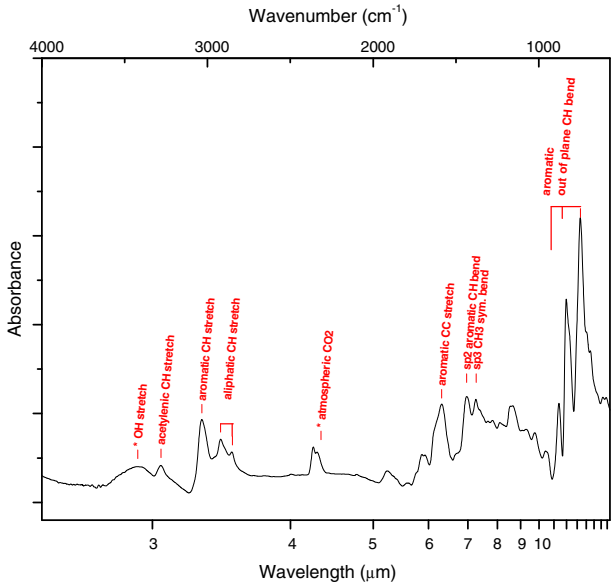

Fig. 4 – Mid resolution (4 cm^{-1}) Fourier transform infrared absorption spectrum of the carbonaceous material mixed with KBr powder and pressed into a pellet.

Table 1 – Identification of the infrared absorption features. The labels S, *m*, and *w* refer respectively to strong, medium, and weak bands while *sh* denotes a shoulder.

ν (cm^{-1})	λ (μm)	Assignment		Rel. abs.
3283	**3.04**	**Alkyne CH stretch**	**S**	
3035	**3.29**	**Aromatic CH stretch**	**S**	**1.000**
2960	**3.38**	**Aliphatic asymmetric CH_3 stretch**	**S**	**0.275**
2920	**3.42**	**Aliphatic asymmetric CH_2 stretch**	**S**	**0.544**
2854	**3.50**	**Aliphatic symmetric CH_2 stretch**	**S**	**0.344**
1916	5.22	Combination of out of plane and in-plane CH bend	*w*	
1706	5.86	Water or carbonyl stretching	*m*	
1687	5.93	Water or carbonyl stretching	*m*	
1625	6.15	Alkene C=C stretch	*sh*	
1586	**6.30**	**Aromatic C=C stretch**	**S**	
1436	6.96	sp^2 aromatic CH bend	*m*	
1380	7.25	sp^3CH_3 symmetric bend	*m*	
1308	7.65	C–C and C–H plane deformation of aromatic groups	*w*	
1280	7.81	Alkene=C–H stretch	*w*	
1235	8.10	Alkene = C–H stretch	*w*	
1173	8.53	Aromatic CH bending in-plane and ring torsion	*w*	
1160	8.62	Aromatic CH in-plane bend	*w*	
1074	9.31	Aromatic CH in-plane bend and ring torsion	*w*	
1023	9.78	Aromatic CH in-plane bend and ring torsion	*w*	
958	10.44	Aromatic CH in-plane bend and ring torsion	*w*	
880	**11.36**	**Aromatic CH out of plane bend for non-adjacent peripheral H atoms**	**S**	
835	**11.98**	**Aromatic CH out of plane bend for two adjacent peripheral H atoms**	**S**	
751	**13.31**	**Aromatic CH out of plane bend for 3–4 adjacent peripheral H atoms**	**S**	
711	14.06	Aromatic CH out of plane bend	*sh*	
689	14.51	Aromatic CH out of plane bend	*sh*	

On the red wing of the OH stretch band, which finds its origin in the presence of atmospheric water adsorbed in the sample, the spectrum shows a small band centered at 3.04 μm (3283 cm^{-1}) assigned to the acetylenic CH stretch. The potential identification of C≡C bonds containing species in the NMR spectrum, although weak, supports this finding. The acetylenic CH stretch is usually detected in the absorption spectrum of soots. Acetylene absorption is also observed in the spectrum of the central star of proto-planetary nebulae [40]. It can be reasonably assumed that interstellar UV irradiation converts acetylenic groups into aromatic structures. The absorption of energetic photons may lead to the homolytic cleavage of one of the C≡C bonds to generate a pair of radicals, known to react rapidly.

We first focus our analysis of the prominent 3.3–3.5 μm region. A spline fitting is performed for determining the baseline. Once the baseline subtracted, the CH stretch absorption feature is deconvoluted into individual components including symmetric and asymmetric aliphatic stretches and aromatic stretch, following the approach described by Dartois et al. for a:C–H [35]. The integrated absorbance of each vibrational mode of specific hydrogen configurations is extracted following this procedure and given in Table 1. It is assumed that partial absorbances are proportional to hydrogen configurations contributing to a particular mode. Quantitative studies of the absorption strength of CH vibrations conducted by Ristein et al., established reliable cross sections for the different CH groups in amorphous carbon material [39]. In order to determine the relative aromatic to aliphatic and $-CH_2$ to $-CH_3$ ratio in our material, we sum the respective symmetric and asymmetric contributions when both partake in the infrared spectrum and obtain the integrated absorbance per CH_2 and CH_3 groups. This methodology leads to derive an aromatic to aliphatic ratio of 3.2:1 for the whole sample. This value is very close to what is found for evolved soots produced in an inverse diffusion flame [38]. We did not proceed to an extraction to separate soluble and insoluble phases. However, information on the chemical structure of the residue can be obtained by combining NMR and IR results. Proton NMR which probes the soluble fraction (about 80% of the total mass) revealed that it was mainly composed of aromatics most probably of low mass. It is well known that molecular size and polarity are factors that affect solubility. For instance, it is expected that small aromatic molecules will dissolve in chloroform better than very large aromatic molecules with substituted alkyl groups. Our IR spectroscopy setup explores the bulk sample. Assuming 3 to 5 H per aromatic ring and 2–3 H per aliphatic group, one can derive an aromatic to aliphatic group ratio of roughly ~1:4 for the residue based on the NMR aromatic to aliphatic hydrogen ratio and the IR aromatic to aliphatic group ratio. These findings suggest that the condensates are composed of aromatic -aliphatic linked hydrocarbon units embedded by low-mass aromatics. Our results are consistent with the findings of Jäger et al. [41] who determined that particles formed by cw laser pyrolysis of C_2H_4 at 1000 K and 1500 K are composed of wt. 100 and 33% of low-mass aromatics. According to the same study, the spectral positions of the infrared features of the extract and the residue are very close (a few wavenumbers). The major difference is the collapse of the CH stretch (3.3 μm) and CH out of plane bending (11–14 μm) absorption bands relative to the CC stretch absorption band. This behavior is expected

because the H/C ratio for small aromatics in the soluble component is larger than for aromatic aliphatic linked structures in the residue.

The aliphatic component is characterized by a CH_2:CH_3 ratio of 2.5:1. As Dartois recalls [42], infrared spectroscopy studies of hydrogen-rich photo-produced or plasma-generated a-C:H usually reveal a CH_2:CH_3 ratio around 2.

The spotlights recently moved to the C=C aromatic stretch, whose spectral position has been proposed as a tracer of the carbon skeleton. According to Pino, it reflects an evolution of the environment of the aromatic units embedded in an aliphatic network [22]. An aromatic sample will show a band at 6.2 μm whereas aliphatic groups attached to aromatic rings will redshift the spectral feature to 6.3 μm. The analysis of our spectrum shows that the band peaks at 6.30 μm with a shoulder at lower wavelength around 6.15 μm. The chemical structure of our sample is therefore close to intermediate stages of evolution of soots produced in, for instance, acetylene rich, low pressure, flat premixed flames [22]. The high initial aliphatic content has been progressively converted into an aliphatic/aromatic network. The final stage being a complete aromatization of the material. The aromatic units are likely stacked and bridged by the numerous aliphatic groups revealed by the infrared spectrum. This conclusion is supported by X-ray diffraction results presented in Section 3.3.

The 6.6–10 μm spectral region (1000–1500 cm^{-1}), which reflects the activity of the CH bending motions and C–C stretching motions, is highly congested on our spectrum. In particular, no structured feature in the 7.6–7.9 μm region comes out of the massif. This is contrasting with infrared spectra of young soot particles which display a strong absorption band at 7.87 μm (1270 cm^{-1}) [38]. This is even more striking when comparing with astronomical observations which show an intense emission feature arising at 7.8 μm in PNe and 7.6 μm in the interstellar medium. Some efforts have recently been engaged to use this feature to trace the evolution of aromatic nanograins [43].

On our spectrum, only two bands can be clearly distinguished at 6.96 and 7.25 μm (1436 and 1380 cm^{-1}) which we assign tentatively to the sp^2 aromatic CH and sp^3 CH_3 symmetric bending modes based on the extensive study of Ristein et al. [39]. The blue wing asymmetry of the 6.96 μm (1436 cm^{-1}) feature may be caused by the contribution resulting from the overlap of bands corresponding to sp^3 CH_3 asymmetric (1470 cm^{-1}) and sp^3 CH_2 (1450 cm^{-1}) bending motions. The spectrum departs from a:C–H material fingerprints for which the 3.4 μm absorption band is accompanied by both 6.85 μm (1460 cm^{-1}) and 7.25 μm (1380 cm^{-1}) features with variable relative intensity ratio [35]. This is consistent with a multi-phase condensate composed of a significant fraction of non-substituted aromatics carrying the 3.29 μm (3035 cm^{-1}) and 6.96 μm (1436 cm^{-1}) features and of aromatic aliphatic linked islands contributing to the 3.4–3.5 μm and 7.25 μm (1380 cm^{-1}) bands.

The 11–15 μm spectral region is sensitive to the aromatic ring edge structures i.e., the number of adjacent peripheral C atoms bonded to an H atom [38,44]. It is generally considered that for regular PAHs, the IR activity in the 11.1–11.6 μm is due to aromatic CH groups which have no neighboring CH groups (dubbed *solo*). Similarly, two, three, and four adjacent CH groups on the edge of the molecular structure will respectively show some activity in the 11.6–12.5, 12.4–13.3, and 13–13.6 μm spectral domains. Based on these considerations which do not take into account the possible substitution of hydrogen atoms by aliphatic groups, the feature at 11.36 μm is tentatively assigned to the solo CH out of plane motion, whereas the band at 11.98 μm is attributed to duo CH bending motion. Solo-CH groups commonly characterize long straight molecular edges, while duets and trios reflect corners. The lack of additional information leads to assign the 13.31 μm to trio and quartet CH bending modes. Laboratory experiments on the spectroscopy of large neutral aromatics show that the absorption cross section per hydrogen of the solo CH mode is six times higher than for the duo CCH bending mode and about twice the cross section for the quartet mode [44]. Our measurements reveal a 11.36 μm feature at least two times smaller than the 11.98 μm feature and three times less intense than the 13.31 μm band. This indicates that duo modes dominate the 11–15 μm region activity suggesting the presence of aromatics with compact structures such as coronene which has only doubly adjacent H atoms on its edge. The activity of the 13.31 μm mode may indicate some pendant rings attached to the structure (four adjacent H atoms) or/and the presence of bays (three adjacent H).

3.3. *X-ray diffraction*

X-ray diffraction is commonly used to characterize the structural details of solid-state substances. It may be a powerful technique for studying disordered materials which are inherently heterogeneous, yielding an estimation of average property. Carbon material powder diffraction data were recorded with a Philips X'Pert X-ray diffractometer using Cu Kα radiation ($\lambda(K\alpha_1)$ = 1.54056 Å, $\lambda(K\alpha_2)$ = 1.54439 Å, 40 kV, 30 mA). The sample was scanned in a step-scan mode (0.017°/step) over the angular range (2θ) of 5–80°. X-ray diffraction data were collected for 1 s at each step. The broad peaks and the diffused nature of the diffraction pattern, displayed in Fig. 5, indicate the presence of a short-range order due to a very small crystallite size.

Similar diffraction profiles have been obtained for amorphous carbon [45] and coal [46]. The three diffraction lines were fitted by a pseudo-Voigt function and the baseline was modeled by a 7-points Bezier function. The most realistic interpretation of the pattern is made on the profile analysis of the second diffraction line only, i.e., the most intense peak, on the assumption that it corresponds to the (0 0 2) reflection of hexagonal graphite. It is assumed than the peak position reflects the average distance between graphene layers and is estimated as 3.98 Å. The high inter-plane value, compared to the average distance between layers in hexagonal graphite which is 3.35 Å, finds its origin in the microstructure of the sample. Let us consider the Debye's equation of the scattered intensity from any atoms in random orientations

$$I_{eu} = \sum_{i,j} f_i f_j \frac{\sin 2\pi s r_{ij}}{2\pi s r_{ij}} \quad (1)$$

where I is expressed in electron units, f is the atomic scattering factor, r_{ij} is the distance of atom pairs i and j, and $s = \frac{2\sin\theta}{\lambda}$.

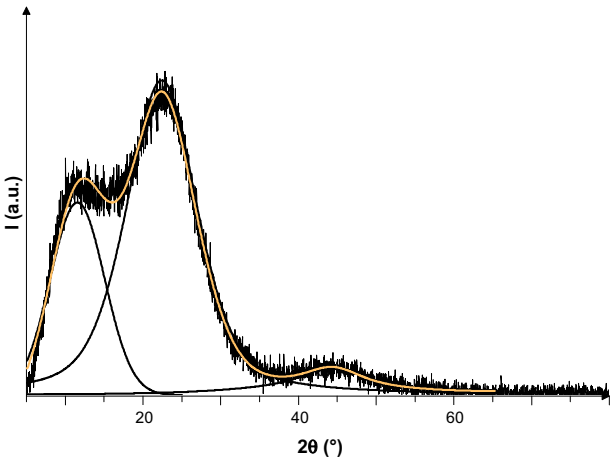

Fig. 5 – X-ray powder pattern of the carbon material after subtraction of the background modeled by a 7-points Bezier function. The three diffraction lines are fitted by a pseudo-Voigt function.

Warren and Bodenstein [47] extended Eq. (1) to *M* sheets of parallel carbon layers, expressed as a two terms equation, i.e., the sum over atoms within a layer *p* (intra-layer interactions) and the sum over the *M* layers (interlayer interactions)

$$I_{eu} = \sum_{p}\sum_{i,j} f_i f_j \frac{\sin 2\pi s r_{ij}}{2\pi s r_{ij}} + \sum_{p}\sum_{p'\neq p}\sum_{i,j} f_i f_j \frac{\sin 2\pi s r_{ij}}{2\pi s r_{ij}} \quad (2)$$

Considering the *M* identical layers,

$$I' = I_{eu}/M = \sum_{i,j} f_i f_j \frac{\sin 2\pi s r_{ij}}{2\pi s r_{ij}} + 2\sum_{p}\left(1-\frac{p}{M}\right)\sum_{i,j} f_i f_j \frac{\sin 2\pi s r_{ij}}{2\pi s r_{ij}} \quad (3)$$

In the case of a small crystallite size, i.e., reduced number of stacking layers, the first intra-layer interactions term cannot be neglected with regard to the second term. As a result, the scattering intensity at small angle range is so strong that the (0 0 2) peak position shifts towards lower angles [47]. This overestimation is commonly accepted in amorphous materials, liquids or gases with very small coherent domains. Indeed, it is a widespread method to approximate the most frequent occurrence of particular inter-atomic or inter-molecular distances by the expression $x_m = \frac{K\lambda}{2\sin\theta_m}$, where x_m denotes the pair distance at the maximum intensity. *K* should admit a value comprised between 1 and 1.3. It is directly derived from the first maximum of the function $\frac{\sin 2\pi s r_{ij}}{2\pi s r_{ij}}$, which gives $s_m = \frac{1.23}{x_m} = \frac{2\sin\theta_m}{\lambda}$, with θ_m the position of the maximum peak height, and $K = 1.23$ in this theoretical interpretation. Such approximate value cannot be used in the particular case of non-spherical shape molecules. A rough crystallite dimension along the *c*-axis, L_c, can be estimated by applying the Scherrer equation:

$$L_c = \frac{\lambda}{\beta(2\theta)\cos\theta} \quad (4)$$

where $\beta(2\theta)$ is the integral breadth of the (0 0 2) diffraction line. Considering the width of the broad peak compared to the instrumental resolution function, the integral breadth was estimated without deconvolution of the profile function. This relationship leads to an average apparent crystallite dimension along the *c*-axis, L_c of the order of 6.5 Å, corresponding to about 2 stacked graphene layers. As a comparison, seventy packed layers characterize high purity synthetic graphite.

Recently published studies may help to assess our conclusions. In particular, simulations of X-ray patterns using the general Debye equation show that the diffraction angle of the (0 0 2) peak decreases and the FWHM of (0 0 2) line increases with decreasing crystallite size for both hexagonal graphite and turbostratic carbon [48,49]. Turbostratic carbon is made of stacked graphene layers randomly folded or crumpled together. The diffraction angles and FWHMs are strongly influenced by the distortion factors, such as the size and microstructure of a crystallite, including disordered stacking of graphene layers, increased interlayer spacing at the edges of flakes or curved graphene layers. They therefore cannot be simply used to characterize the lattice parameters and crystallite size of turbostratic carbon. This finding is of consequence here because we cannot exclude that the layers are not stacked regularly as in hexagonal graphite. The crystallite dimension has then to be considered cautiously. Nevertheless, pattern modeling of nanoparticles obtained from hydrated cerium oxides with very small crystallite diameters (~10 Å) showed results similar to us in terms of simulated FWHMs [50].

The diffraction feature observed on the left-hand side of the (0 0 2) peak centered at $2\theta = 11.4°$ cannot be decisively assigned. A so called γ band is observed for instance in coals but at a somewhat larger angle $2\theta = 18°$. The relative intensity of the γ feature with the (0 0 2) peak has been used as a tracer for aromaticity [51]. It is interpreted as the presence of aliphatic side chains (or condensed saturated rings) grafted on the edge of the graphene layer. Although one cannot exclude the presence of grafted structures on the graphene, the high intensity of this peak on our spectrum is rather mainly attributed to inter-particle scattering by close-packed particles and small angle scattering by cracks, micropores and other heterogeneities present in the sample. The wide-angle peak on the profile with a maximum at $2\theta = 44.28°$ emerges close to the (1 0 0) and (1 0 1) three dimensional diffraction lines of hexagonal graphite, onto which is superposed the two dimensional (1 0) line of the same material. Considering the possible contribution of several bands to the diffraction peak and its low intensity, this part of the profile was not used to extract information on the crystallite size along the *a*-axis, as explained above.

Based on the sole analysis of the (0 0 2) diffraction peak, we were able to reveal the presence of double graphene layers in the carbon material produced at 1400 K. It may also contain large amounts of single aromatic layers but only methods such as HRTEM dark field diffraction mode may help us to refine our description. Experiments of laser pyrolysis of butadiene (C_4H_6) reveal that a raise in the temperature of formation generates a structural transition from an amorphous-like carbon to a polyaromatic turbostratic carbon [52]. Below 1300 K, images recorded by high resolution Transmission Electron Microscopy through an absorption contrast suggest that the layers are mainly single (non-stacked) [28]. Thanks to the combination of IR spectroscopy and HRTEM imaging, Herlin and co-workers were able to establish a relationship between the mean layer size and the intensity ratio between the 11.36 and 13.31 μm (880 and 751 cm^{-1}) infrared bands.

4. Conclusion

We have shown that an original porous graphite reactor can be successfully used to produce carbonaceous particles by pyrolysis of acetylene. The physical and chemical conditions under which pyrolytic carbons are synthesized in our reactor bear some resemblance with circumstellar environments. For instance, the innermost region (between 1 and 5 stellar radii) of the circumstellar shell of the brightest carbon star, IRC+10216, is characterized by a temperature that declines from 2300 to 900 K and a gas number density that falls from 10^{16} to 10^{9} molecule/cm^3 when going away from the star [53]. Recent observations have put some constraint on the acetylene abundance at the 7.5×10^{-6} level [54] which confirm the importance of this molecular precursor. Oxygen is supposedly not participating in the carbon particle chemistry in carbon rich shells as it is locked up in CO. This is also the case in our reactor in which only acetylene is injected. In circumstellar environments, the temperature controls the reactivity and the physical growth of the particle whereas the number of collisions modulates the growth yield. The dynamics of the shell sets the time scale. Shock waves produced by pulsations of the star and propagating outwards will also affect the chemistry. These effects are far from being well understood but overall reduce the time available while simultaneously boost the density enhancing collisions. Considering the similarities while keeping in mind differences (i.e., in terms of dynamics), the reactor appears as a promising tool to explore some aspects of the formation of analogues of circumstellar particles under physical and chemical conditions reasonably close to those found in carbon rich circumstellar shells.

The particles have been probed by ex situ methods of proton NMR spectroscopy, FT-IR spectroscopy and X-ray diffraction. Despite the limited number of techniques used, a wealth of information has been obtained. The proton NMR analysis reveals that the soluble component (about wt. 80%) is composed mainly of small aromatics (in a 8.1:1 ratio). This is consistent with earlier studies that show that low temperature pyrolysis (below 1500 K) produces particles composed of low mass PAHs [29,41]. The absence of olefinic protons confirms the evolutionary stage of this phase of the carbon material.

Infrared spectroscopy which probes the bulk sample shows that the overall aromatic to aliphatic ratio is ~3.2 to 1 through the analysis of the 3.4 μm region. By combining IR and NMR, we can access some information on the chemical structure of the residue (wt. 20%). In particular, we derive an approximate aromatic to aliphatic ratio of 1:4 which is distinct from the soluble component. It is consistent with a structure of aromatic aliphatic linked hydrocarbon material.

The absorption spectrum bears some strong similarities with some selected spectral windows of astronomical emission spectra of post AGB stars. Several of them exhibit the 3.4 and 6.3 μm features typical of aliphatic containing material. The comparison of infrared emission spectrum with gas and/or solid phases absorption spectra should be done carefully when considering relative intensities, band profiles and precise band peak positions. The analysis of the emission and absorption spectra of a selection of neutral and ionized PAHs, shows for instance a shift of the band peak position arising from the departure from the harmonic oscillator model of the highly excited vibrational modes [55]. Global spectral trends of laboratory absorption and IR emission spectra seem however to follow similar trends (see [55] and references therein).

The spectral diversity of the unidentified infrared emission bands has resulted in their classification into three major groups: A, B and C [56,57] characterized by the frequency of the CC stretching mode. A variety of astrophysical objects falls in the class A category whereas class C sources are less frequent. Recently Pino et al. suggested that the frequency of the CC mode traces the aromatic to aliphatic ratio [22]. The carriers of class C infrared emission spectra are proposed to be dominated by aliphatic branches linking aromatic units embedded within the network. At the end of the evolution, class A spectra correspond to more matured structures in which aliphatics have been converted into aromatic cycles. Class B sources are intermediate cases. In the light of the aromatic to aliphatic ratio and the position of the CC stretching 6.30 μm band, the laboratory analogues find themselves at the transition from class C to class B carriers. Completing this picture, we have extracted a CH_2:CH_3 ratio about 2.5 that corresponds to the right window for growth of a stable network [42].

The X-ray analysis points towards a mostly amorphous chemical structure that contains small organized aromatic islands composed of typically two graphene layers and bridged by aliphatic groups. Because of possible multiple contributions, we were unable to retrieve the crystallite dimension along the *a*-axis in the plane of the graphene layer but the broadness of the peak suggests very small sizes.

The condensate is composed of small crystalline aromatic aliphatic linked units surrounded by low-mass aromatics. This investigation pinpoints the stage of evolution of the carbon material which appears to be at an intermediate level where plenty of aliphatic branches in the core have just started to convert to aromatic units and well before graphene layer in-plane growth and stacking. We believe that this work complements existing studies on the characterization of circumstellar analogues of carbon dust particles. Future work will aim to investigate the chemical and physical properties of the particles produced under varying conditions (precursor gas, temperature, etc.). For instance, it would be interesting to determine how the increase in temperature leads to the production of fullerene containing particles [58] and if chemical intermediates can be identified. The infrared spectral fingerprints of the carbon material will be recorded for detailed comparison with astronomical spectra. It would be very valuable to investigate the effects of thermal and photo-processing of the sample. For this purpose, some other methods such as Transmission Electron Microscopy are envisaged. In parallel, we are currently working on a modified design that would allow high temperature kinetics studies of some of the key species involved in the formation of the particles. Future plans include in situ mass spectrometry and laser induced spectroscopy probes.

Acknowledgments

The authors would like to acknowledge funding from the Indo-French Centre for the Promotion of Advanced Research (Project Number 3405-3). This work is also supported by the

French Programmes of "Physique Stellaire" and of "Physique et Chimie du Milieu Interstellaire". We are grateful to Jonathan Thiévin for its participation in the characterization of the source, Ragavendra Balakrishna for his help in recording the high resolution emission spectra of acetylene, and Emmanuel Dartois and Thomas Pino for fruitful discussions that helped in understanding the absorption infrared spectrum of the material. Finally we thank the anonymous referees who greatly helped improving the manuscript.

REFERENCES

[1] Gillett FC, Forrest WJ, Merrill KM. 8–13 μm spectra of NGC-7027, BD+30° 3639, and NGC-6572. Astrophys J 1973;183(1):87–93.
[2] Léger A, Puget JL. Identification of the unidentified IR emission features of interstellar dust. Astron. Astrophys 1984;137(1):L5–8.
[3] Allamandola LJ, Tielens A, Barker JR. Polycyclic aromatic-hydrocarbons and the unidentified infrared-emission bands – auto exhaust along the milky-way. Astrophys J 1985;290(1):L25–8.
[4] Allamandola LJ, Tielens A, Barker JR. Interstellar polycyclic aromatic-hydrocarbons – the infrared-emission bands, the excitation emission mechanism, and the astrophysical implications. Astrophysical Journal Suppl Ser 1989;71(4):733–75.
[5] Borghesi A, Bussoletti E, Colangeli L. Amorphous-carbon and the unidentified infrared bands. Astrophys J 1987;314(1):422–8.
[6] Papoular R, Conard J, Giuliano M, Kister J, Mille G. A coal model for the carriers of the unidentified IR bands. Astron Astrophys 1989;217(1–2):204–8.
[7] Sakata A, Wada S, Tanabe T, Onaka T. Infrared-spectrum of the laboratory-synthesized quenched carbonaceous composite (QCC) – comparison with the infrared unidentified emission bands. Astrophys J 1984;287(1):L51–4.
[8] Frenklach M, Feigelson ED. Formation of polycyclic aromatic-hydrocarbons in circumstellar envelopes. Astrophys J 1989;341(1):372–84.
[9] Cherchneff I, Barker JR, Tielens A. Polycyclic aromatic hydrocarbon formation in carbon-rich stellar envelopes. Astrophys J 1992;401(1):269–87.
[10] Cherchneff I. Forming dust precursors in the inner envelopes of carbon-rich AGB stars. Astrophys Space Sci 1995; 224(1–2):379–82.
[11] Cherchneff I. Chemical models of AGB winds. Mol Astrophys: Probes Processes 1997:469–75.
[12] Cadwell BJ, Wang H, Feigelson ED, Frenklach M. Induced nucleation of carbon dust in red giant stars. Astrophys J 1994;429(1):285–99.
[13] Frenklach M. Reaction mechanism of soot formation in flames. Phys Chem Chem Phys 2002;4(11): 2028–37.
[14] Sabbah H, Biennier L, Sims I, Rowe BR. Exploring the role of PAHs in the formation of soot: the reaction of dimerization of pyrene, in preparation.
[15] Morgan WA, Feigelson ED, Wang H, Frenklach M. A new mechanism for the formation of meteoritic kerogen-like material. Science 1991;252(5002):109–12.
[16] D'Anna A, D'Alessio A, Minutolo P. Spectroscopic and chemical characterization of soot inception processes in premixed laminar flames at atmospheric pressure. In: Bockhorn H, editor. Soot formation in combustion. Berlin, Heidelberg: Springer Verlag; 1994. p. 83–103.
[17] Dobbins RA, Subramaniasivam H. Soot precursor particles in flames. In: Bockhorn H, editor. Soot formation in combustion. Berlin, Heidelberg: Springer Verlag; 1994. p. 290–301.
[18] Siegmann K, Sattler K, Siegmann HC. Clustering at high temperatures: carbon formation in combustion. J Electron Spectrosc Relat Phenom 2002;126(1–3):191–202.
[19] Reilly PTA, Gieray RA, Whitten WB, Ramsey JM. Direct observation of the evolution of the soot carbonization process in an acetylene diffusion flame via real-time aerosol mass spectrometry. Combust Flame 2000;122(1–2):90–104.
[20] Grotheer H-H, Hoffmann K, Wolf K, Kanjarkar S, Wahl C, Aigner M. Study of carbonaceous nanoparticles in premixed C_2H_4-air flames and behind a spark ignition engine. Combust Flame 2009;156(4):791–800.
[21] D'Anna A. Combustion-formed nanoparticles. Proc Combust Inst 2009;32(1):593–613.
[22] Pino T, Dartois E, Cao A-T, Carpentier Y, Chamaillé T, Vasquez R, et al. The 6.2 μm band position in laboratory and astrophysical spectra: a tracer of the aliphatic to aromatic evolution of interstellar carbonaceous dust. Astron Astrophys 2008;490:665–72.
[23] Jones AP. Carbon-atom clusters in random covalent networks – PAHs as an integral component of interstellar HAC. Mon Not Roy Astron Soc 1990;247(2):305–10.
[24] Kwok S, Volk K, Bernath P. On the origin of infrared plateau features in proto-planetary nebulae. Astrophys J 2001;554(1):L87–90.
[25] Buchta C, Dalessio A, Danna A, Gambi G, Minutolo P, Russo S. The optical characterization of high-molecular-mass carbonaceous structures produced in premixed laminar flames across the soot threshold limit. Planet Space Sci 1995;43(10–11):1227–32.
[26] Mennella V, Colangeli L, Bussoletti E. The absorption-coefficient of cosmic carbon analog grains in the wavelength range 20–2000 μm. Astron Astrophys 1995;295(1): 165–70.
[27] Schnaiter M, Henning T, Mutschke H, Kohn B, Ehbrecht M, Huisken F. Infrared spectroscopy of nano-sized carbon grains produced by laser pyrolysis of acetylene: analog materials for interstellar grains. Astrophys J 1999;519(2):687–96.
[28] Galvez A, Herlin-Boime N, Reynaud C, Clinard C, Rouzaud JN. Carbon nanoparticles from laser pyrolysis. Carbon 2002;40(15):2775–89.
[29] Jäger C, Krasnokutski S, Staicu A, Huisken F, Mutschke H, Henning T, et al. Identification and spectral properties of polycyclic aromatic hydrocarbons in carbonaceous soot produced by laser pyrolysis. Astrophys J Suppl Ser 2006;166(2):557–66.
[30] Goto M, Maihara T, Terada H, Kaito C, Kimura S, Wada S. Infrared spectral sequence of quenched carbonaceous composite subjected to thermal annealing. Astron Astrophys Suppl Ser 2000;141(1):149–56.
[31] Furton DG, Laiho JW, Witt AN. The amount of interstellar carbon locked in solid hydrogenated amorphous carbon. Astrophys J 1999;526(2):752–63.
[32] Scott A, Duley WW. The decomposition of hydrogenated amorphous carbon: a connection with polycyclic aromatic hydrocarbon molecules. Astrophys J 1996;472(2):L123–5.
[33] Mennella V, Brucato JR, Colangeli L, Palumbo P. Activation of the 3.4 μm band in carbon grains by exposure to atomic hydrogen. Astrophys J 1999;524(1):L71–4.
[34] Kroto HW, Heath JR, O'Brien SC, Curl RF, Smalley RE. C_{60}: buckminsterfullerene. Nature 1985;318(6042):162–3.
[35] Dartois E, Caro GMM, Deboffle D, d'Hendecourt L. Diffuse interstellar medium organic polymers – photoproduction of the 3.4, 6.85 and 7.25 μm features. Astron Astrophys 2004;423(3):L33–6.

[36] Thiévin J, Georges R, Carles S, Benidar A, Rowe B, Champion JP. High-temperature emission spectroscopy of methane. J Quant Spectrosc Radiat Transfer 2008;109(11):2027–36.
[37] Mendiara T, Domene MP, Millera A, Bilbao R, Alzueta MU. An experimental study of the soot formed in the pyrolysis of acetylene. J Anal Appl Pyrolysis 2005;74(1–2):486–93.
[38] Santamaría A, Mondragón F, Molina A, Marsh ND, Eddings EG, Sarofim AF. FT-IR and ^{1}H NMR characterization of the products of an ethylene inverse diffusion flame. Combust Flame 2006;146(1–2):52–62.
[39] Ristein J, Stief RT, Ley L, Beyer W. A comparative analysis of a-C:H by infrared spectroscopy and mass selected thermal effusion. J Appl Phys 1998;84(7):3836–47.
[40] Goto M, Gaessler W, Hayano Y, Iye M, Kamata Y, Kanzawa T, et al. Spatially resolved 3 μm spectroscopy of IRAS 22272+5435: formation and evolution of aliphatic hydrocarbon dust in proto-planetary nebulae. Astrophys J 2003;589(1):419–29.
[41] Jäger C, Huisken F, Mutschke H, Jansa IL, Henning TH. Formation of polycyclic aromatic hydrocarbons and carbonaceous solids in gas-phase condensation experiments. Astrophys J 2009;696(1):706–12.
[42] Dartois E, Caro GMM, Deboffle D, Montagnac G, d'Hendecourt L. Ultraviolet photoproduction of ISM dust – laboratory characterisation and astrophysical relevance. Astron Astrophys 2005;432(3):895–908.
[43] Joblin C, Szczerba R, Berné O, Szyszka C. Carriers of the mid-IR emission bands in PNe reanalysed evidence of a link between circumstellar and interstellar aromatic dust. Astron Astrophys 2008;490(1):189–96.
[44] Hony S, Van Kerckhoven C, Peeters E, Tielens A, Hudgins DM, Allamandola LJ. The CH out-of-plane bending modes of PAH molecules in astrophysical environments. Astron Astrophys 2001;370(3):1030–43.
[45] Sarkar A, Dasgupta K, Barat P, Mukherjee P, Sathiyamoorthy D. Studies on neon irradiated amorphous carbon using X-ray diffraction technique. Int J Mod Phys B 2008;22(7):865–75.
[46] Cook DJ, Schlemmer S, Balucani N, Wagner DR, Harrison JA, Steiner B, et al. Single photon infrared emission spectroscopy: a study of IR emission from UV laser excited PAHs between 3 and 15 μm. J Phys Chem A 1998;102(9):1465–81.
[47] Warren BE, Bodenstein P. The diffraction pattern of fine particle carbon blacks. Acta Crystallogr 1965;18:282–6.
[48] Fujimoto H. Theoretical X-ray scattering intensity of carbons with turbostratic stacking and AB stacking structures. Carbon 2003;41(8):1585–92.
[49] Whitesides R, Kollias AC, Domin D, Lester WA, Frenklach M. Graphene layer growth: collision of migrating five-member rings. Proc Combust Inst 2007;31:539–46.
[50] Audebrand N, Auffrédic J-P, Louër D. An X-ray powder diffraction study of the microstructure and growth kinetics of nanoscale crystallites obtained from hydrated cerium oxides. Chem Mater 2000;12(6):1791–9.
[51] Yen TF, Erdman JG, Pollack SS. Investigation of the structure of petroleum asphaltenes by X-ray diffraction. Anal Chem 1961;33(11):1587–94.
[52] Herlin N, Bohn I, Reynaud C, Galvez A, Rouzaud JN. Nanoparticles produced by laser pyrolysis of hydrocarbons: analogy with carbon cosmic dust. Astron Astrophys 1998;330(3):1127–35.
[53] Fonfria JP, Cernicharo J, Richter MJ, Lacy JH. A detailed analysis of the dust formation zone of IRC+10216 derived from mid-infrared bands of C_2H_2 and HCN. Astrophys J 2008;673(1):445–69.
[54] Agundez M, Cernicharo J. Oxygen chemistry in the circumstellar envelope of the carbon-rich star IRC+10216. Astrophys J 2006;650(1):374–93.
[55] Tielens A. Interstellar polycyclic aromatic hydrocarbon molecules. Annu Rev Astron Astrophys 2008;46:289–337.
[56] Peeters E, Hony S, Van Kerckhoven C, Tielens A, Allamandola LJ, Hudgins DM, et al. The rich 6–9 μm spectrum of interstellar PAHs. Astron Astrophys 2002;390(3):1089–113.
[57] van Diedenhoven B, Peeters E, Van Kerckhoven C, Hony S, Hudgins DM, Allamandola LJ, et al. The profiles of the 3–12 μm polycyclic aromatic hydrocarbon features. Astrophys J 2004;611(August 1):928–39.
[58] Jäger C, Mutschke H, Henning T, Huisken F. Spectral properties of gas-phase condensed fullerene-like carbon nanoparticles from far-ultraviolet to infrared wavelengths. Astrophys J 2008;689(December 1):249–59.